Commun. Comput. Phys.
doi: 10.4208/cicp.110711.170212a

Vol. **13**, No. 2, pp. 442-460
February 2013

A Two-Parameter Continuation Method for Rotating Two-Component Bose-Einstein Condensates in Optical Lattices

Y.-S. Wang[1], B.-W. Jeng[2] and C.-S. Chien[3,*]

[1] *Department of Applied Mathematics, National Chung Hsing University, Taichung 402, Taiwan.*
[2] *Department of Mathematics Education, National Taichung University of Education, Taichung 403, Taiwan.*
[3] *Department of Computer Science and Information Engineering, Ching Yun University, Jungli 320, Taiwan.*

Received 11 July 2011; Accepted (in revised version) 17 February 2012

Available online 28 June 2012

Abstract. We study efficient spectral-collocation and continuation methods (SCCM) for rotating two-component Bose-Einstein condensates (BECs) and rotating two-component BECs in optical lattices, where the second kind Chebyshev polynomials are used as the basis functions for the trial function space. A novel two-parameter continuation algorithm is proposed for computing the ground state and first excited state solutions of the governing Gross-Pitaevskii equations (GPEs), where the classical tangent vector is split into two constraint conditions for the bordered linear systems. Numerical results on rotating two-component BECs and rotating two-component BECs in optical lattices are reported. The results on the former are consistent with the published numerical results.

AMS subject classifications: 65N35, 35P30, 35Q55

Key words: Spectral collocation method, second kind Chebyshev polynomials, periodic potential, bifurcation.

1 Introduction

Quantized vortex lattices in a rotating Bose-Einstein condensate (BEC) have been observed experimentally in the past decade [1–4]. Since then the study of quantized vortices plays a key role in superfluidity and superconductivity. While many interesting

*Corresponding author. *Email addresses:* wang04.wang25@msa.hinet.net (Y.-S. Wang), bwjeng@mail.ntcu.edu.tw (B.-W. Jeng), cschien@cyu.edu.tw, cschien@amath.nchu.edu.tw (C.-S. Chien)

phenomena have been observed in single rotating component BEC [1–4], it is expected that a rich variety of static and dynamic phenomena will be found in rotating two component BECs. In this paper, we impose the effect of optical lattices on the physical system. At extremely low temperature, the mathematical model of rotating two-component BECs in optical lattices is described by the macroscopic wave functions $\Psi_j(\mathbf{x},t)$ $(j=1,2)$ whose evolution is governed by the coupled Gross-Pitaevskii equations (GPEs):

$$\mathbf{i}\frac{\partial}{\partial t}\Psi_j=-\frac{1}{2}\Delta\Psi_j+V(\mathbf{x})\Psi_j+P(\mathbf{x})\Psi_j+\left(\sum_{l=1}^{2}\eta_{jl}|\Psi_l|^2\right)\Psi_j-\omega L_z\Psi_j,\qquad \mathbf{x}\in\Omega\subset\mathbb{R}^2, \tag{1.1a}$$

$$\Psi_j(\mathbf{x},t)=0,\qquad t\geq 0,\quad \mathbf{x}\in\partial\Omega,\quad j=1,2, \tag{1.1b}$$

where $V(\mathbf{x})=(\gamma_x^2x^2+\gamma_y^2y^2)/2$ is the trapping potential with γ_x and γ_y the trap frequencies in the x- and y- direction, respectively, $P(\mathbf{x})=a_1\sin^2(\pi x/d_1)+a_2\sin^2(\pi y/d_2)$ is the periodic potential with a_1 and a_2 the recoil energies, and d_1 and d_2 are the distance between neighbor wells (lattice constants) in the x- and y- axis, respectively, $\Omega\subset\mathbb{R}^2$ is a bounded domain with piecewise smooth boundary $\partial\Omega$, ω is an angular velocity, and $L_z=xp_y-yp_x=-\mathbf{i}(x\partial y-y\partial x)$ is the z-component of the angular momentum $L=\mathbf{x}\times P$ with the momentum operator $P=-\mathbf{i}\nabla=(p_x,p_y,p_z)^T$. The intra-component interactions and inter-component interactions in the two-component BECs are represented by η_{jj} $(j=1,2)$ and η_{jl} $(j\neq l,\ j,l=1,2)$ respectively. An important invariant of the GPEs is the normalization of the wave functions

$$\int_\Omega|\Psi_j(\mathbf{x},t)|^2d\mathbf{x}=1,\qquad j=1,\ 2,\quad t\geq 0. \tag{1.2}$$

Mueller and Ho [5] investigated the vortex lattice structure of (1.1) by assuming the lowest Landau level approximation and a perfect lattice. Kasamatsu *et al*. [6, 7] studied the vortex states structure of (1.1) with equal intra-component interaction strengths $\eta_{11}=\eta_{22}$ by varying the inter-component interaction constants η_{12} and η_{21} [7]. They also studied vortex states with and without internal Josephson coupling [8]. Recently, they studied the vortex sheet structure in rotating immiscible two-component BECs [9]. Zhang *et al*. studied the dynamics of (1.1) both analytically and numerically [10]. Recently, Wang studied numerical simulations for computing the ground state solutions of (1.1) [11].

Substituting the formula

$$\Psi_j(\mathbf{x},t)=e^{-\mathbf{i}\lambda_jt}\psi_j(\mathbf{x}),\qquad j=1,2,$$

into (1.1), we obtain a system of two stationary state nonlinear eigenvalue problems

$$\lambda_j\psi_j(\mathbf{x})=-\frac{1}{2}\Delta\psi_j(\mathbf{x})+V(\mathbf{x})\psi_j(\mathbf{x})+P(\mathbf{x})\psi_j(\mathbf{x})+\left(\sum_{l=1}^{2}\eta_{jl}|\psi_l(\mathbf{x})|^2\right)\psi_j(\mathbf{x})$$
$$-\omega L_z\psi_j(\mathbf{x}),\qquad \mathbf{x}\in\Omega, \tag{1.3a}$$

$$\psi_j(\mathbf{x})=0,\quad \text{on }\partial\Omega,\quad j=1,2, \tag{1.3b}$$

where λ_j are the chemical potential associated with the complex wave functions $\psi_j(\mathbf{x})$, $j=1,2$. In this paper, we study spectral collocation methods (SCM) combined with a two-parameter continuation algorithm for computing the ground state and first excited state solutions of (1.1), where the second kind Chebyshev polynomials described in [12] are used as the basis functions for the trial function space. Also see [13] for a more recent monograph on spectral methods. We will follow the first two solution curves of (1.1) as in [14–17]. That is, we will use the first two minimal eigenvalues of the linear eigenvalue problem associated with (1.3) as initial guesses to approximate the counterparts of (1.3). The constraint condition (1.2) is used as a target point in the curve-tracking. We stop the curve-tracking whenever the target point is reached. Since the two components ψ_1 and ψ_2 represent two different matters, the associated chemical potentials λ_1 and λ_2 should be different. The discretization of (1.3) is a system of nonlinear equations involving state variables ψ_1, ψ_2, and parameters λ_1 and λ_2.

We recall in differential topology the normalization of a tangent vector is called a parametrization via arc length, which is used as the constraint condition in the continuation method, and plays a key role as the normalization of the wave functions (1.2). Our aim here is to propose a two-parameter continuation algorithm for computing numerical solutions of (1.3), where the chemical potentials λ_1 and λ_2 are treated as the continuation parameters simultaneously. Since both λ_1 and λ_2 play the same role in the physical system, the constraint conditions for the bordered linear systems used in the continuation method should be equally chosen. Instead of using (1.2) as the second constraint condition [18], we split the tangent vector $(\dot{\psi}_1,\dot{\psi}_2,\dot{\lambda}_1,\dot{\lambda}_2)^T$ into two constraint conditions, namely, $(\dot{\psi}_1,0,\dot{\lambda}_1,0)^T$ and $(0,\dot{\psi}_2,0,\dot{\lambda}_2)^T$ for the bordered linear systems. To the best of our knowledge, the numerical study of rotating two-component BECs in optical lattices has never been reported in the literature.

This paper is organized as follows. In Section 2 we use the second kind Chebyshev polynomials to study the SCM for (1.1). In Section 3 we describe a two-parameter continuation algorithm for computing numerical solutions of (1.1). The numerical results are reported in Section 4. Finally, some concluding remarks are given in Section 5.

2 A SCM method using the second kind Chebyshev polynomials

We express the complex functions $\psi_j(\mathbf{x})$ in (1.3), $j=1,2$, as $\psi_1(\mathbf{x})=u_R(\mathbf{x})+\mathbf{i}u_T(\mathbf{x})$ and $\psi_2(\mathbf{x})=v_R(\mathbf{x})+\mathbf{i}v_T(\mathbf{x})$, where $u_R(\mathbf{x})$, $u_T(\mathbf{x})$, $v_R(\mathbf{x})$ and $v_T(\mathbf{x})$ are real functions. Thus (1.3) becomes a real system of four nonlinear GPEs, which are expressed as

$$-\frac{1}{2}\Delta u_R+Vu_R+Pu_R+\left[\eta_{11}(u_R^2+u_T^2)+\eta_{12}(v_R^2+v_T^2)\right]u_R \\ +\omega\left(-x(u_T)_y+y(u_T)_x\right)=\lambda_1 u_R, \qquad \text{in } \Omega, \tag{2.1a}$$

$$-\frac{1}{2}\Delta u_T + Vu_T + Pu_T + \left[\eta_{11}(u_R^2+u_T^2)+\eta_{12}(v_R^2+v_T^2)\right]u_T + \omega\left(x(u_R)_y - y(u_R)_x\right) = \lambda_1 u_T, \qquad \text{in } \Omega, \tag{2.1b}$$

$$-\frac{1}{2}\Delta v_R + Vv_R + Pv_R + \left[\eta_{21}(u_R^2+u_T^2)+\eta_{22}(v_R^2+v_T^2)\right]v_R + \omega\left(-x(v_T)_y + y(v_T)_x\right) = \lambda_2 v_R, \qquad \text{in } \Omega, \tag{2.1c}$$

$$-\frac{1}{2}\Delta v_T + Vv_T + Pv_T + \left[\eta_{21}(u_R^2+u_T^2)+\eta_{22}(v_R^2+v_T^2)\right]v_T + \omega\left(x(v_R)_y - y(v_R)_x\right) = \lambda_2 v_T, \qquad \text{in } \Omega, \tag{2.1d}$$

$$u_R(\mathbf{x}) = u_T(\mathbf{x}) = v_R(\mathbf{x}) = v_T(\mathbf{x}) = 0, \qquad \text{on } \partial\Omega, \tag{2.1e}$$

where $(u_R)_x$, $(u_T)_x$, $(v_R)_x$, $(v_T)_x$ and $(u_R)_y$, $(u_T)_y$, $(v_R)_y$, $(v_T)_y$ denote the partial derivatives of u_R, u_T, v_R, and v_T with respect to x and y, respectively.

The second kind Chebyshev polynomials was first used in [16] for computing symmetry-breaking solutions of the GPE. In this section we study spectral collocation methods using the same basis functions for numerical solutions of (1.1). Similar to using Fourier sine functions as the basis functions for the spectral method [17], the second kind Chebyshev polynomials also can supply accurate numerical solutions for the GPE with exponential rate of convergence [16]. Let $U_k(x)$ be the second kind Chebyshev polynomial of degree k, which is defined as

$$U_k(x) = \frac{\sin(k+1)\theta}{\sin\theta} \quad \text{when } x=\cos\theta, \quad \theta\in[0,\pi] \iff x\in[-1,1], \quad k=1,2,3,\cdots.$$

Let S_N^1 be the subspace spanned by $\{U_0(x), U_1(x), \cdots, U_N(x)\}$. We choose the trial function space V_N^1 as

$$V_N^1 = \{v\in S_N^1 : v(\pm 1) = 0\}.$$

Since $U_k(\pm 1) = (\pm 1)^k(k+1)$, it is clear that the functions $U_k(x)$ do not satisfy the boundary conditions of the GPE. Thus we construct a set of basis functions $\phi_k(x)$ for V_N^1 by setting

$$\phi_k(x) = \frac{U_k(x)}{k+1} - \frac{U_{k+2}(x)}{k+3}, \qquad k=0,1,\cdots,N-2.$$

It follows that $\phi_k(x)\in V_N^1$ and $\{\phi_k(x)\}_{k=0}^{N-2}$ are linearly independent. Thus $V_N^1 = \text{span}\{\phi_0(x), \phi_1(x), \cdots, \phi_{N-2}(x)\}$ with $\dim V_N^1 = N-1$.

Let $V_N^2 = \text{span}\{\phi_k(x)\phi_j(y) : k,j=0,1,\cdots,N-2\}$ be the 2D trial function space. We choose the roots of the second kind Chebyshev polynomials as the collocation points. The SCM for solving (2.1) is to find the approximate solutions

$$u_R^N(x,y) = \sum_{k,j=0}^{N-2} \alpha_{kj}\phi_k(x)\phi_j(y) \in V_N^2, \qquad u_T^N(x,y) = \sum_{k,j=0}^{N-2} \beta_{kj}\phi_k(x)\phi_j(y) \in V_N^2, \tag{2.2a}$$

$$v_R^N(x,y) = \sum_{k,j=0}^{N-2} \gamma_{kj}\phi_k(x)\phi_j(y) \in V_N^2, \qquad v_T^N(x,y) = \sum_{k,j=0}^{N-2} \delta_{kj}\phi_k(x)\phi_j(y) \in V_N^2, \tag{2.2b}$$

such that

$$-\frac{1}{2}\Delta u_R^N(x_l,y_m)+[V(x_l,y_m)+P(x_l,y_m)-\lambda_1]u_R^N(x_l,y_m)+\Big[\eta_{11}\big((u_R^N)^2(x_l,y_m)+(u_T^N)^2(x_l,y_m)\big)$$
$$+\eta_{12}\Big((v_R^N)^2(x_l,y_m)+(v_T^N)^2(x_l,y_m)\Big)\Big]u_R^N(x_l,y_m)+\omega\Big[-x_l(u_T^N)_y+y_m(u_T^N)_x\Big]=0, \tag{2.3a}$$

$$-\frac{1}{2}\Delta u_T^N(x_l,y_m)+[V(x_l,y_m)+P(x_l,y_m)-\lambda_1]u_T^N(x_l,y_m)+\Big[\eta_{11}\big((u_R^N)^2(x_l,y_m)+(u_T^N)^2(x_l,y_m)\big)$$
$$+\eta_{12}\Big((v_R^N)^2(x_l,y_m)+(v_T^N)^2(x_l,y_m)\Big)\Big]u_T^N(x_l,y_m)+\omega\Big[x_l(u_R^N)_y-y_m(u_R^N)_x\Big]=0, \tag{2.3b}$$

$$-\frac{1}{2}\Delta v_R^N(x_l,y_m)+[V(x_l,y_m)+P(x_l,y_m)-\lambda_2]v_R^N(x_l,y_m)+\Big[\eta_{21}\big((u_R^N)^2(x_l,y_m)+(u_T^N)^2(x_l,y_m)\big)$$
$$+\eta_{22}\Big((v_R^N)^2(x_l,y_m)+(v_T^N)^2(x_l,y_m)\Big)\Big]v_R^N(x_l,y_m)+\omega\Big[-x_l(v_T^N)_y+y_m(v_T^N)_x\Big]=0, \tag{2.3c}$$

$$-\frac{1}{2}\Delta v_T^N(x_l,y_m)+[V(x_l,y_m)+P(x_l,y_m)-\lambda_2]v_T^N(x_l,y_m)+\Big[\eta_{21}\big((u_R^N)^2(x_l,y_m)+(u_T^N)^2(x_l,y_m)\big)$$
$$+\eta_{22}\Big((v_R^N)^2(x_l,y_m)+(v_T^N)^2(x_l,y_m)\Big)\Big]v_T^N(x_l,y_m)+\omega\Big[x_l(v_R^N)_y-y_m(v_R^N)_x\Big]=0, \tag{2.3d}$$

where $l,m=0,1,\cdots,N-2$. We denote $\phi_{kj}=\phi_j(x_k)$, $\phi'_{kj}=\phi'_j(x_k)$, $\phi''_{kj}=\phi''_j(x_k)$, $v_{lm}=V(x_l,y_m)$, $p_{lm}=P(x_l,y_m)$, and define the matrices

$$\Phi=(\phi_{kj})_{0\le k,j\le N-2},\quad \Phi'=(\phi'_{kj})_{0\le k,j\le N-2},\quad \Phi''=(\phi''_{kj})_{0\le k,j\le N-2},$$
$$V=\mathrm{diag}(v_{0,0},v_{1,0},\cdots,v_{N-2,0},v_{0,1},v_{1,1},\cdots,v_{N-2,1},\cdots,v_{N-2,N-2}),$$
$$P=\mathrm{diag}(p_{0,0},p_{1,0},\cdots,p_{N-2,0},p_{0,1},p_{1,1},\cdots,p_{N-2,1},\cdots,p_{N-2,N-2}),$$
$$I_{(N-1)^2}\in\mathbb{R}^{(N-1)^2\times(N-1)^2}\text{ is the identity matrix, and}$$
$$X=\mathrm{diag}(x_0,x_1,\cdots,x_{N-2}),\qquad Y=\mathrm{diag}(y_0,y_1,\cdots,y_{N-2}).$$

Let "$\otimes$" and "$\circ$" denote the matrix tensor product and the vector Hadamard product, respectively. For any vector $\boldsymbol{v}\in\mathbb{R}^n$, we define $\boldsymbol{v}^{②}=\boldsymbol{v}\circ\boldsymbol{v}$. Denote

$$\tilde{\alpha}=(\alpha_{0,0},\alpha_{1,0},\cdots,\alpha_{N-2,0},\alpha_{0,1},\alpha_{1,1},\cdots,\alpha_{N-2,1},\cdots,\alpha_{N-2,N-2})^T,$$
$$\tilde{\beta}=(\beta_{0,0},\beta_{1,0},\cdots,\beta_{N-2,0},\beta_{0,1},\beta_{1,1},\cdots,\beta_{N-2,1},\cdots,\beta_{N-2,N-2})^T,$$
$$\tilde{\gamma}=(\gamma_{0,0},\gamma_{1,0},\cdots,\gamma_{N-2,0},\gamma_{0,1},\gamma_{1,1},\cdots,\gamma_{N-2,1},\cdots,\gamma_{N-2,N-2})^T,$$
$$\tilde{\delta}=(\delta_{0,0},\delta_{1,0},\cdots,\delta_{N-2,0},\delta_{0,1},\delta_{1,1},\cdots,\delta_{N-2,1},\cdots,\delta_{N-2,N-2})^T.$$

The SCM analogue of (2.1) is a nonlinear system of equations involving parameters λ_1 and λ_2 and is given as

$$F(\tilde{\alpha},\tilde{\beta},\tilde{\gamma},\tilde{\delta},\lambda_1,\lambda_2)=\begin{bmatrix}F_1(\tilde{\alpha},\tilde{\beta},\tilde{\gamma},\tilde{\delta},\lambda_1,\lambda_2)\\F_2(\tilde{\alpha},\tilde{\beta},\tilde{\gamma},\tilde{\delta},\lambda_1,\lambda_2)\\F_3(\tilde{\alpha},\tilde{\beta},\tilde{\gamma},\tilde{\delta},\lambda_1,\lambda_2)\\F_4(\tilde{\alpha},\tilde{\beta},\tilde{\gamma},\tilde{\delta},\lambda_1,\lambda_2)\end{bmatrix}=0, \tag{2.4}$$

where $F:\mathbb{R}^{4(N-1)^2}\times\mathbb{R}^2\to\mathbb{R}^{4(N-1)^2}$ is a smooth mapping with

$$\begin{aligned}
&F_1(\tilde{\alpha},\tilde{\beta},\tilde{\gamma},\tilde{\delta},\lambda_1,\lambda_2)\\
=&-\frac{1}{2}(\Phi\otimes\Phi''+\Phi''\otimes\Phi)\tilde{\alpha}+(V+P-\lambda_1 I_{(N-1)^2})(\Phi\otimes\Phi)\tilde{\alpha}\\
&+\Big\{\eta_{11}\big[((\Phi\otimes\Phi)\tilde{\alpha})^{②}+((\Phi\otimes\Phi)\tilde{\beta})^{②}\big]+\eta_{12}\big[((\Phi\otimes\Phi)\tilde{\gamma})^{②}+((\Phi\otimes\Phi)\tilde{\delta})^{②}\big]\Big\}(\Phi\otimes\Phi)\tilde{\alpha}\\
&+\omega\big[-(I_{N-1}\otimes X)(\Phi'\otimes\Phi)\tilde{\beta}+(Y\otimes I_{N-1})(\Phi\otimes\Phi')\tilde{\beta}\big], \qquad (2.5a)\\
&F_2(\tilde{\alpha},\tilde{\beta},\tilde{\gamma},\tilde{\delta},\lambda_1,\lambda_2)\\
=&-\frac{1}{2}(\Phi\otimes\Phi''+\Phi''\otimes\Phi)\tilde{\beta}+(V+P-\lambda_1 I_{(N-1)^2})(\Phi\otimes\Phi)\tilde{\beta}\\
&+\Big\{\eta_{11}\big[((\Phi\otimes\Phi)\tilde{\alpha})^{②}+((\Phi\otimes\Phi)\tilde{\beta})^{②}\big]+\eta_{12}\big[((\Phi\otimes\Phi)\tilde{\gamma})^{②}+((\Phi\otimes\Phi)\tilde{\delta})^{②}\big]\Big\}(\Phi\otimes\Phi)\tilde{\beta}\\
&+\omega\big[(I_{N-1}\otimes X)(\Phi'\otimes\Phi)\tilde{\alpha}-(Y\otimes I_{N-1})(\Phi\otimes\Phi')\tilde{\alpha}\big], \qquad (2.5b)\\
&F_3(\tilde{\alpha},\tilde{\beta},\tilde{\gamma},\tilde{\delta},\lambda_1,\lambda_2)\\
=&-\frac{1}{2}(\Phi\otimes\Phi''+\Phi''\otimes\Phi)\tilde{\gamma}+(V+P-\lambda_2 I_{(N-1)^2})(\Phi\otimes\Phi)\tilde{\gamma}\\
&+\Big\{\eta_{21}\big[((\Phi\otimes\Phi)\tilde{\alpha})^{②}+((\Phi\otimes\Phi)\tilde{\beta})^{②}\big]+\eta_{22}\big[((\Phi\otimes\Phi)\tilde{\gamma})^{②}+((\Phi\otimes\Phi)\tilde{\delta})^{②}\big]\Big\}(\Phi\otimes\Phi)\tilde{\gamma}\\
&+\omega\big[-(I_{N-1}\otimes X)(\Phi'\otimes\Phi)\tilde{\delta}+(Y\otimes I_{N-1})(\Phi\otimes\Phi')\tilde{\delta}\big], \qquad (2.5c)\\
&F_4(\tilde{\alpha},\tilde{\beta},\tilde{\gamma},\tilde{\delta},\lambda_1,\lambda_2)\\
=&-\frac{1}{2}(\Phi\otimes\Phi''+\Phi''\otimes\Phi)\tilde{\delta}+(V+P-\lambda_2 I_{(N-1)^2})(\Phi\otimes\Phi)\tilde{\delta}\\
&+\Big\{\eta_{21}\big[((\Phi\otimes\Phi)\tilde{\alpha})^{②}+((\Phi\otimes\Phi)\tilde{\beta})^{②}\big]+\eta_{22}\big[((\Phi\otimes\Phi)\tilde{\gamma})^{②}+((\Phi\otimes\Phi)\tilde{\delta})^{②}\big]\Big\}(\Phi\otimes\Phi)\tilde{\delta}\\
&+\omega\big[(I_{N-1}\otimes X)(\Phi'\otimes\Phi)\tilde{\gamma}-(Y\otimes I_{N-1})(\Phi\otimes\Phi')\tilde{\gamma}\big]. \qquad (2.5d)
\end{aligned}$$

For simplicity, we let

$$\begin{aligned}
&\boldsymbol{u}_1=[\tilde{\alpha}^T,\tilde{\beta}^T]^T, \qquad \boldsymbol{u}_2=[\tilde{\gamma}^T,\tilde{\delta}^T]^T, \qquad E=-\frac{1}{2}(\Phi\otimes\Phi''+\Phi''\otimes\Phi),\\
&G=\Phi\otimes\Phi, \qquad W=\omega\big[-(I_{N-1}\otimes X)(\Phi'\otimes\Phi)+(Y\otimes I_{N-1})(\Phi\otimes\Phi')\big].
\end{aligned}$$

And (2.5) is simplified as

$$\begin{aligned}
F_1(\boldsymbol{u}_1,\boldsymbol{u}_2,\lambda_1,\lambda_2)=&E\tilde{\alpha}+(V+P-\lambda I_{(N-1)^2})G\tilde{\alpha}+\Big\{\eta_{11}\big[(G\tilde{\alpha})^{②}+(G\tilde{\beta})^{②}\big]\\
&+\eta_{12}\big[(G\tilde{\gamma})^{②}+(G\tilde{\delta})^{②}\big]\Big\}G\tilde{\alpha}+W\tilde{\beta}, \qquad (2.6a)\\
F_2(\boldsymbol{u}_1,\boldsymbol{u}_2,\lambda_1,\lambda_2)=&E\tilde{\beta}+(V+P-\lambda I_{(N-1)^2})G\tilde{\beta}+\Big\{\eta_{11}\big[(G\tilde{\alpha})^{②}+(G\tilde{\beta})^{②}\big]\\
&+\eta_{12}\big[(G\tilde{\gamma})^{②}+(G\tilde{\delta})^{②}\big]\Big\}G\tilde{\beta}-W\tilde{\alpha}, \qquad (2.6b)
\end{aligned}$$

$$F_3(\boldsymbol{u}_1,\boldsymbol{u}_2,\lambda_1,\lambda_2)=E\tilde{\gamma}+(V+P-\lambda I_{(N-1)^2})G\tilde{\gamma}+\Big\{\eta_{21}\big[(G\tilde{\alpha})^{②}+(G\tilde{\beta})^{②}\big]$$
$$+\eta_{22}\big[(G\tilde{\gamma})^{②}+(G\tilde{\delta})^{②}\big]\Big\}G\tilde{\gamma}+W\tilde{\delta}, \tag{2.6c}$$
$$F_4(\boldsymbol{u}_1,\boldsymbol{u}_2,\lambda_1,\lambda_2)=E\tilde{\delta}+(V+P-\lambda I_{(N-1)^2})G\tilde{\delta}+\Big\{\eta_{21}\big[(G\tilde{\alpha})^{②}+(G\tilde{\beta})^{②}\big]$$
$$+\eta_{22}\big[(G\tilde{\gamma})^{②}+(G\tilde{\delta})^{②}\big]\Big\}G\tilde{\delta}-W\tilde{\gamma}. \tag{2.6d}$$

The Jacobian matrix $DF=[D_{\boldsymbol{u}_1}F,D_{\boldsymbol{u}_2}F,D_{\lambda_1}F,D_{\lambda_2}F]\in\mathbb{R}^{4(N-1)^2\times(4(N-1)^2+2)}$ is a block matrix of the following form

$$DF=\begin{bmatrix} L_1+M_{11} & W+\eta_{11}M_{12} & \eta_{12}M_{13} & \eta_{12}M_{14} & -G\tilde{\alpha} & 0\\ -W+\eta_{11}M_{12} & L_1+M_{22} & \eta_{12}M_{23} & \eta_{12}M_{24} & -G\tilde{\beta} & 0\\ \eta_{21}M_{13} & \eta_{21}M_{23} & L_2+M_{33} & W+\eta_{22}M_{34} & 0 & -G\tilde{\gamma}\\ \eta_{21}M_{14} & \eta_{21}M_{24} & -W+\eta_{22}M_{34} & L_2+M_{44} & 0 & -G\tilde{\delta} \end{bmatrix},$$

where

$$L_1=E+(V+P-\lambda_1 I_{(N-1)^2})G,\qquad L_2=E+(V+P-\lambda_2 I_{(N-1)^2})G,$$
$$M_{11}=\Big[3\eta_{11}\mathrm{diag}((G\tilde{\alpha})^{②})+\eta_{11}\mathrm{diag}((G\tilde{\beta})^{②})+\eta_{12}\mathrm{diag}((G\tilde{\gamma})^{②})+\eta_{12}\mathrm{diag}((G\tilde{\delta})^{②})\Big]G,$$
$$M_{22}=\Big[\eta_{11}\mathrm{diag}((G\tilde{\alpha})^{②})+3\eta_{11}\mathrm{diag}((G\tilde{\beta})^{②})+\eta_{12}\mathrm{diag}((G\tilde{\gamma})^{②})+\eta_{12}\mathrm{diag}((G\tilde{\delta})^{②})\Big]G,$$
$$M_{33}=\Big[\eta_{21}\mathrm{diag}((G\tilde{\alpha})^{②})+\eta_{21}\mathrm{diag}((G\tilde{\beta})^{②})+3\eta_{22}\mathrm{diag}((G\tilde{\gamma})^{②})+\eta_{22}\mathrm{diag}((G\tilde{\delta})^{②})\Big]G,$$
$$M_{44}=\Big[\eta_{21}\mathrm{diag}((G\tilde{\alpha})^{②})+\eta_{21}\mathrm{diag}((G\tilde{\beta})^{②})+\eta_{22}\mathrm{diag}((G\tilde{\gamma})^{②})+3\eta_{22}\mathrm{diag}((G\tilde{\delta})^{②})\Big]G,$$
$$M_{12}=2\mathrm{diag}(G\tilde{\alpha})\mathrm{diag}(G\tilde{\beta})G,\qquad M_{13}=2\mathrm{diag}(G\tilde{\alpha})\mathrm{diag}(G\tilde{\gamma})G,$$
$$M_{14}=2\mathrm{diag}(G\tilde{\alpha})\mathrm{diag}(G\tilde{\delta})G,\qquad M_{23}=2\mathrm{diag}(G\tilde{\beta})\mathrm{diag}(G\tilde{\gamma})G,$$
$$M_{24}=2\mathrm{diag}(G\tilde{\beta})\mathrm{diag}(G\tilde{\delta})G,\qquad M_{34}=2\mathrm{diag}(G\tilde{\gamma})\mathrm{diag}(G\tilde{\delta})G.$$

We will incorporate the SCM in a predictor-corrector continuation algorithm, and obtain the spectral-collocation and continuation algorithm (SCCM), which will be used to compute the ground state as well as first excited state solutions of the GPEs, where the block GMRES cited in [19] will be used as the linear solver.

3 A two-parameter continuation algorithm

During the past years, various numerical continuation algorithms have been proposed [20–26] for computing numerical solutions of the GPE, or the so-called nonlinear Schrödinger equation (NLS). In particular, Chen *et al*. [22] used the coupling coefficient as the continuation parameter in the context of a predictor-corrector continuation algorithm for computing the ground states and excited states of spin-1 BEC. In this section, we will

use the chemical potential as the continuation parameter. Then the eigenvalues of the associated linear Schrödinger equation (LS) are just bifurcation points of the NLS on the trivial solution curve $\{(0,0,\lambda_1,\lambda_2)|\lambda_1,\lambda_2\in\mathbb{R}^+\}$. To compute the ground state and first excited-state solutions of the GPE, we use a predictor-corrector continuation algorithm to trace the solution curves branching from the first two minimal eigenvalues of the LS. We stop the curve-tracking whenever the constraint condition (1.2) is satisfied. That is, we use the energy levels and wave functions of the LS as initial guesses to approximate the counterparts of the NLS. The main purpose of this section is to describe a two-parameter continuation algorithm for computing the ground state and first excited state solutions of rotating two-component BECs and rotating two-component BECs in optical lattices. The nonlinear systems of equations (2.4) can be expressed as

$$F(\boldsymbol{u}_1,\boldsymbol{u}_2,\lambda_1,\lambda_2)=0, \tag{3.1}$$

where $F:\mathbb{R}^{4(N-1)^2}\times\mathbb{R}^2\to\mathbb{R}^{4(N-1)^2}$ is a smooth mapping with $\boldsymbol{u}_1=[\tilde{\alpha}^T,\tilde{\beta}^T]^T\in\mathbb{R}^{2(N-1)^2}$, $\boldsymbol{u}_2=[\tilde{\gamma}^T,\tilde{\delta}^T]^T\in\mathbb{R}^{2(N-1)^2}$, λ_1, $\lambda_2\in\mathbb{R}$. We denote the Jacobian matrix of the operator F by $DF=[D_{\boldsymbol{u}_1}F,D_{\boldsymbol{u}_2}F,D_{\lambda_1}F,D_{\lambda_2}F]$, where $A=[D_{\boldsymbol{u}_1}F,D_{\boldsymbol{u}_2}F]$ is the linearization of the mapping F at the equilibrium $\boldsymbol{u}_1^0=\boldsymbol{u}_2^0=[0,\cdots,0]^T\in\mathbb{R}^{2(N-1)^2}$, i.e.,

$$\begin{aligned}[D_{\boldsymbol{u}_1}F,D_{\boldsymbol{u}_2}F](0,0,\lambda_1,\lambda_2)&=\begin{bmatrix} L_1 & W & 0 & 0\\ -W & L_1 & 0 & 0\\ 0 & 0 & L_2 & W\\ 0 & 0 & -W & L_2\end{bmatrix}\\ &=K-\lambda_1\begin{bmatrix} G & 0 & 0 & 0\\ 0 & G & 0 & 0\\ 0 & 0 & 0 & 0\\ 0 & 0 & 0 & 0\end{bmatrix}-\lambda_2\begin{bmatrix} 0 & 0 & 0 & 0\\ 0 & 0 & 0 & 0\\ 0 & 0 & G & 0\\ 0 & 0 & 0 & G\end{bmatrix},\end{aligned}$$

where

$$K=\begin{bmatrix} E+VG & W & 0 & 0\\ -W & E+VG & 0 & 0\\ 0 & 0 & E+VG & W\\ 0 & 0 & -W & E+VG\end{bmatrix},$$

and L_1, L_2, W, E, V, G are defined in Section 2. We recall that the number of linearly independent eigenvectors associated with an eigenvalue λ is called the geometric multiplicity of λ. Denote the geometric multiplicity and algebraic multiplicity of λ by $\rho(\lambda)$ and $\sigma(\lambda)$, respectively. We have the following result.

Lemma 3.1. *All the eigenvalues of the matrix K are at least quadruple.*

Proof. Let $[\alpha_1^T,\beta_1^T,\gamma_1^T,\delta_1^T]^T$ be an eigenvector of K associated with the eigenvalue λ which satisfies $\beta_1^T\alpha_1\delta_1^T\gamma_1\neq0$ and $\beta_1^T\gamma_1-\alpha_1^T\delta_1\neq0$. Note that $\alpha_1,\beta_1,\gamma_1,\delta_1\in\mathbb{R}^{(N-1)^2\times1}$. It is clear that

$[-\alpha_1,-\beta_1,\gamma_1,\delta_1]^T$, $[\gamma_1,\delta_1,\alpha_1,\beta_1]^T$, and $[\gamma_1,\delta_1,-\alpha_1,-\beta_1]^T$ are also eigenvectors of K associated with λ. Since these eigenvectors are linearly independent, the geometric multiplicity $\rho(\lambda)$ of λ is 4. Since $\rho(\lambda)<\sigma(\lambda)$ [27, p. 316], the result follows immediately. □

Denote the solution curves of (3.1) by

$$c=\{y(s)=(\boldsymbol{u}_1(s),\boldsymbol{u}_2(s),\lambda_1(s),\lambda_2(s))^T|F(y(s))=0,s\in I\},$$

where I is any interval in $\mathbb{R}^1$. Assuming that a parametrization via arc length is available on c, we will trace the solution curve c by predictor-corrector continuation methods [28,29]. Let $y^{(i)}=(\boldsymbol{u}_1^{(i)},\boldsymbol{u}_2^{(i)},\lambda_1^{(i)},\lambda_2^{(i)})^T\in\mathbb{R}^{4(N-1)^2+2}$ be a point which has been accepted as an approximating point for c, and $\dot{y}^{(i)}=(\dot{\boldsymbol{u}}_1^{(i)},\dot{\boldsymbol{u}}_2^{(i)},\dot{\lambda}_1^{(i)},\dot{\lambda}_2^{(i)})^T\in\mathbb{R}^{4(N-1)^2+2}$ be a tangent vector to c at $y^{(i)}$. Since the two components of the BECs have different physical properties, the associated chemical potentials λ_1 and λ_2 should be treated as the continuation parameters simultaneously. Instead of implementing the classical predictor-corrector continuation methods, we propose a novel two-parameter continuation algorithm as follows. We split the tangent vector $\dot{y}^{(i)}$ into $\dot{y}^{(i)}=\dot{y}_1^{(i)}+\dot{y}_2^{(i)}$, where $\dot{y}_1^{(i)}=(\dot{u}_1^{(i)},0,\dot{\lambda}_1^{(i)},0)^T$ and $\dot{y}_2^{(i)}=(0,\dot{u}_2^{(i)},0,\dot{\lambda}_2^{(i)})^T$. Next, we set $||\dot{y}_1^{(i)}||=||\dot{y}_2^{(i)}||=1$. A new point $z^{(i+1,1)}$ is predicted by the Euler predictor

$$z^{(i+1,1)}=y^{(i)}+\delta^{(i)}v^{(i)},$$

where $\delta^{(i)}>0$ is the step length, and $v^{(i)}$ is the unit tangent vector at $y^{(i)}$, which is obtained by solving the linear system

$$\begin{bmatrix} D_{\boldsymbol{u}_1}F(y^{(i)}) & D_{\boldsymbol{u}_2}F(y^{(i)}) & D_{\lambda_1}F(y^{(i)}) & D_{\lambda_2}F(y^{(i)}) \\ \dot{\boldsymbol{u}}_1^{(i-1)} & 0 & \dot{\lambda}_1^{(i-1)} & 0 \\ 0 & \dot{\boldsymbol{u}}_2^{(i-1)} & 0 & \dot{\lambda}_2^{(i-1)} \end{bmatrix} v^{(i)}=\begin{bmatrix} \tilde{0} \\ \tilde{0} \\ 1 \\ 1 \end{bmatrix}. \tag{3.2}$$

The accuracy of approximation to the solution curve must be improved via a corrector process. In practice, the modified Newton's method with constraint

$$\begin{bmatrix} D_{\boldsymbol{u}_1}F(z^{(i+1,j)}) & D_{\boldsymbol{u}_2}F(z^{(i+1,j)}) & D_{\lambda_1}F(z^{(i+1,j)}) & D_{\lambda_2}F(z^{(i+1,j)}) \\ \dot{\boldsymbol{u}}_1^{(i)} & 0 & \dot{\lambda}_1^{(i)} & 0 \\ 0 & \dot{\boldsymbol{u}}_2^{(i)} & 0 & \dot{\lambda}_2^{(i)} \end{bmatrix} w^{(j)}$$
$$=\begin{bmatrix} -F(z^{(i+1,j)}) \\ 0 \\ 0 \end{bmatrix}, \tag{3.3}$$

is solved, and we set $z^{(i+1,j+1)}=z^{(i+1,j)}+w^{(j)}$, $j=1,2,\cdots$. If $y^{(i)}$ lies sufficiently near c, then the modified Newton's method will converge if the step size $\delta^{(i)}$ is small enough. We

simplify (3.2) or (3.3) as

$$\begin{bmatrix} A & \tilde{p}_1 & \tilde{p}_2 \\ \tilde{q}_1^T & r_1 & 0 \\ \tilde{q}_2^T & 0 & r_2 \end{bmatrix} \begin{bmatrix} \tilde{x} \\ \lambda_1 \\ \lambda_2 \end{bmatrix} = \begin{bmatrix} \tilde{f} \\ g_1 \\ g_2 \end{bmatrix}, \tag{3.4}$$

where

$$A \in \mathbb{R}^{4(N-1)^2 \times 4(N-1)^2}, \quad \tilde{p}_1 = D_{\lambda_1} F(z^{(i+1,j)}), \quad \tilde{p}_2 = D_{\lambda_2} F(z^{(i+1,j)}), \quad \tilde{q}_1 = (\dot{\boldsymbol{u}}_1^{(i)}, 0),$$
$$\tilde{q}_2 = (0, \dot{\boldsymbol{u}}_2^{(i)}), \quad \tilde{f} \in \mathbb{R}^{4(N-1)^2}, \quad r_1 = \dot{\lambda}_1^{(i)}, \quad r_2 = \dot{\lambda}_2^{(i)}, \quad g_1, g_2 \in \mathbb{R}.$$

Note that the block elimination algorithm [30] can be used to solve (3.4), which involves solving linear systems with multiple right hand sides. Thus we can apply the Block GMRES (BGMRES) [19] to solve (3.4).

4 Numerical results

We used the SCCM with $N = 20$ to compute the ground state and first excited state solutions of rotating two-component BECs and rotating two-component BECs in optical lattices, where we chose $V(\mathbf{x}) = (x^2 + y^2)/2$ and $\Omega = (-6,6)^2$ in (1.3). In the captions, $\lambda_{j,1}$ and $\lambda_{j,2}$ denote the first two minimum eigenvalues of the discrete nonlinear eigenvalue problem, $\lambda_{j,1}^*$ and $\lambda_{j,2}^*$ denote the energy levels of the ground state solution and first excited state solution of the j-th component, respectively, and n_j, $j = 1,2$, denote the number of vortices of the wave function $|\psi_j|^2$. The accuracy tolerance for the Newton corrector is 10^{-9}. Let

$$M = \begin{bmatrix} \eta_{11} & \eta_{12} \\ \eta_{21} & \eta_{22} \end{bmatrix} = \eta \cdot \begin{bmatrix} \tilde{\eta}_{11} & \tilde{\eta}_{12} \\ \tilde{\eta}_{21} & \tilde{\eta}_{22} \end{bmatrix}$$

be the interaction matrix, where η_{ij} are defined in (1.1), and $\tilde{\eta}_{ij}$ are approximately normalized to the unit. When $\eta = 10, 10^2, 10^3$, which corresponds to the fact that the particle number of BECs approximately equals to $10^4, 10^5$, and 10^6, respectively. In Examples 4.2-4.3 we studied how the vortices of the two components varied with respect to the angular velocity, and the particle numbers of the BECs. In Examples 4.4-4.5 we studied how the vortices of the two components were affected by the strength of the periodic potential. All computations were executed on an Intel®Core™2 Quad PC using MATLAB.

Example 4.1. The eigenpairs of the linear eigenvalue problem

$$-\Delta u = \lambda u, \qquad \text{in } \Omega = (-1,1)^2, \tag{4.1a}$$
$$u = 0, \qquad \text{on } \partial\Omega, \tag{4.1b}$$

Table 1: The first eigenvalues of (4.1) and the first bifurcation points of (4.2) with respect to various values of N.

	Linear		Nonlinear	
N	eigenvalue	error	bifurcation point	error
4	4.9336434125297322	1.1588E-003	4.9336434105653225	1.1588E-003
6	4.9348156646332884	1.3464E-005	4.9348156646332930	1.3464E-005
8	4.9348021294696700	7.1075E-008	4.9348021294696723	7.1075E-008
10	4.9348022008156356	2.7096E-010	4.9348022008156291	2.7095E-010
12	4.9348022005439454	7.3430E-013	4.9348022005439098	7.6916E-013
14	4.9348022005446754	3.5527E-015	4.9348022005446620	1.6875E-014

are of the following form:

$$\lambda_{m,n}=\frac{(m^2+n^2)\pi^2}{4},$$
$$u_{m,n}(x,y)=\sin\left(\frac{m\pi(x+1)}{2}\right)\sin\left(\frac{n\pi(y+1)}{2}\right),\qquad m,n=1,2,\cdots.$$

In this example, we verified numerically that the convergence rate of the SCM is exponential. We used the SCCM to discretize (4.1), and detected the first bifurcation point of the 2D semilinear elliptic eigenvalue problem [31,32]

$$-\Delta u=\lambda\sinh u,\qquad \text{in } \Omega=(-1,1)^2, \tag{4.2a}$$
$$u=0,\qquad \text{on } \partial\Omega. \tag{4.2b}$$

Eq. (4.2) describes a model for the equilibrium of a set of point vortices or a guiding center plasma in the domain Ω. Table 1 lists the first eigenvalue of (4.1) and (4.2) with $N=$

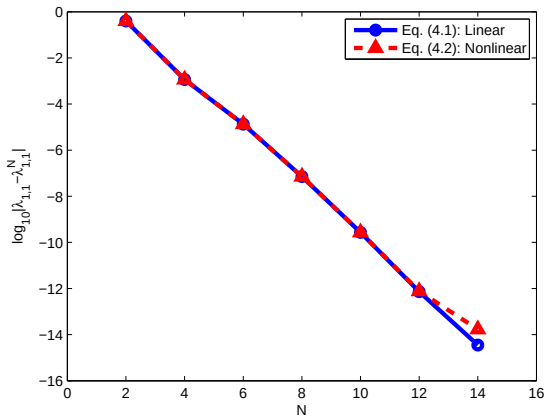

Figure 1: The convergence diagram of the spectral collocation method applied to (4.1) and (4.2), where $\lambda_{1,1}=2\pi^2/4=4.934802200544679$.

4,6,8,10,12,14. Fig. 1 shows how the errors of the spectral collocation method decrease with respect to N, which also shows that the convergence rate is exponential.

Example 4.2 (The ground state solutions of rotating two-component BECs.)**.** We used the SCCM to trace the first solution curves of (1.3) with $P(\mathbf{x})=0$. The following cases were implemented: (i) $\eta_{11}=110$, $\eta_{22}=90$, and $\eta_{12}=\eta_{21}=70$. Note that the matrix $M=(\eta_{ij})$ is symmetric and positive definite, and diagonally dominant. Fig. 2(a) shows the solution curves of the ground state solutions of ψ_1 and ψ_2 with $\omega=0.7$, where $\lambda_{1,1}\approx 1.0001$, $\lambda_{2,1}\approx 1.0001$, $\lambda^*_{1,1}\approx 3.3678$, and $\lambda^*_{2,1}\approx 3.3536$. Fig. 2(b) shows the solution curves of the ground state solutions of ψ_1 and ψ_2 with $\omega=0.85$, where $\lambda_{1,1}\approx 1.0001$, $\lambda_{2,1}\approx 1.0001$, $\lambda^*_{1,1}\approx 3.1094$, and $\lambda^*_{2,1}\approx 3.0538$. Fig. 3 shows that the numbers of vortices of the wave functions $|\psi_1|^2$ and $|\psi_2|^2$ increase with respect to the angular velocity ω. Table 2(a) lists the locations of the first bifurcation points, and the energy levels of the ground state solutions for the wave functions $|\psi_1|^2$ and $|\psi_2|^2$. (ii) We fixed $\omega=0.7$ and chose various scales of coefficients η_{ij}, Fig. 4 shows that the numbers of vortices of the wave functions $|\psi_1|^2$ and $|\psi_2|^2$ increase with respect to the values of the coefficients η_{ij}. Table 2(b) lists the locations of the first bifurcation points, and the energy levels of the ground state solutions for the wave functions $|\psi_1|^2$ and $|\psi_2|^2$.

Table 2: The first bifurcation points and associated energy levels of (1.3) with $P(\mathbf{x})=0$.

(a) $\eta_{11}=110$, $\eta_{22}=90$, $\eta_{12}=\eta_{21}=70$.

ω	0.7	0.85	0.9	0.95
$\lambda_{1,1}=\lambda_{2,1}$	1.0001	1.0001	1.0001	1.0001
$\lambda^*_{1,1}$	3.3678	3.1094	2.6189	2.4085
$\lambda^*_{2,1}$	3.3536	3.0538	2.5755	2.2761
n_1	4	4	8	8
n_2	4	4	4	8

(b) $\omega=0.7$, $\eta_{11}=110$, $\eta_{22}=90$, $\eta_{12}=\eta_{21}=70$.

η_{ij}	$0.5M$	$2M$	$5M$	$10M$
$\lambda_{1,1}=\lambda_{2,1}$	1.0001	1.0001	1.0001	1.0001
$\lambda^*_{1,1}$	2.8126	4.4858	6.7478	9.2885
$\lambda^*_{2,1}$	2.6932	4.4730	6.6491	9.2780
n_1	4	4	8	12
n_2	4	4	8	8

Example 4.3 (The first excited state solutions of rotating two-component BECs.)**.** We used the SCCM to trace the second solution curves of (1.3) with $P(\mathbf{x})=0$. The following cases were implemented: (i) $\eta_{11}=110$, $\eta_{22}=90$, and $\eta_{12}=\eta_{21}=70$. Fig. 5 shows that the numbers of vortices of the wave functions $|\psi_1|^2$ and $|\psi_2|^2$ increase with respect to the angular velocity ω. Table 3(a) lists the locations of the second bifurcation points, and the energy

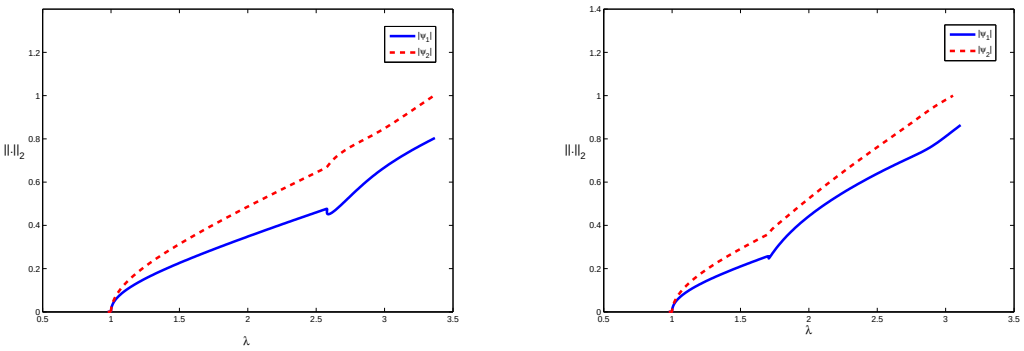

(a) $\omega=0.7$. (b) $\omega=0.85$.

Figure 2: The solution curves of the ground state solutions of (1.3) with $P(\mathbf{x})=0$, where $\eta_{11}=110$, $\eta_{22}=90$, $\eta_{12}=\eta_{21}=70$, and $\omega=0.7$, 0.85.

levels of the first excited state solutions for the wave functions $|\psi_1|^2$ and $|\psi_2|^2$. (ii) We fixed $\omega=0.7$ and chose various scales of coefficients η_{ij}, Fig. 6 shows that the numbers of vortices of the wave functions $|\psi_1|^2$ and $|\psi_2|^2$ increase with respect to the values of the coefficients η_{ij}. Table 3(b) lists the locations of the second bifurcation points, and the energy levels of the first excited state solutions for the wave functions $|\psi_1|^2$ and $|\psi_2|^2$.

Table 3: The second bifurcation points and associated energy levels of (1.3) with $P(\mathbf{x})=0$.

(a) $\eta_{11}=110$, $\eta_{22}=90$, $\eta_{12}=\eta_{21}=70$.

ω	0.7	0.8	0.9	0.95
$\lambda_{1,2}=\lambda_{2,2}$	1.2991	1.1991	1.0991	1.0491
$\lambda^*_{1,2}$	3.3528	3.0375	2.5995	2.2759
$\lambda^*_{2,2}$	3.3494	3.0261	2.5725	2.2551
n_1	5	5	5	9
n_2	1	5	5	9

(b) $\omega=0.7$, $\eta_{11}=110$, $\eta_{22}=90$, $\eta_{12}=\eta_{21}=70$.

η_{ij}	$0.5M$	$2M$	$5M$	$10M$
$\lambda_{1,2}=\lambda_{2,2}$	1.2991	1.2991	1.2991	1.2991
$\lambda^*_{1,2}$	2.6069	4.4612	6.7209	9.2306
$\lambda^*_{2,2}$	2.5785	4.4589	6.6247	9.2207
n_1	1	5	9	13
n_2	1	5	9	9

Example 4.4 (The ground state solutions of rotating two-component BECs in optical lattices.)**.** We used the SCCM to trace the first solution curves of (1.3) where $\omega=0.7$, $\eta_{11}=1100$, $\eta_{22}=900$, $\eta_{12}=\eta_{21}=700$ and $d_1=d_2=d=3$. Fig. 7 shows the peaks of the wave

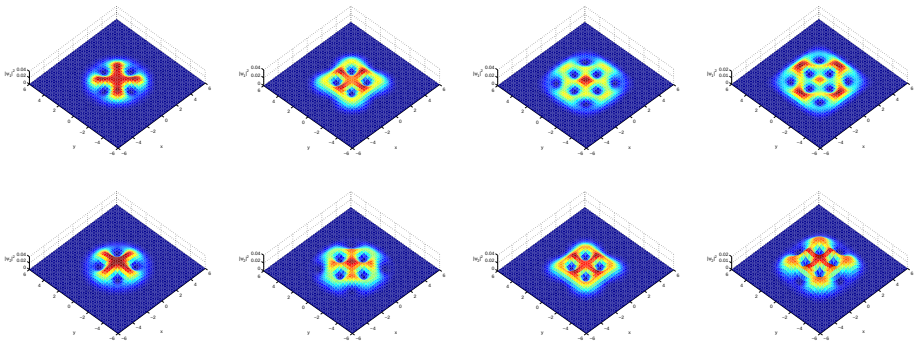

Figure 3: The contours of the ground state solutions of (1.3) with $P(\mathbf{x})=0$, upper: $|\psi_1|^2$, low: $|\psi_2|^2$, where $\omega=0.7$, 0.85, 0.9, and 0.95, $\eta_{11}=110$, $\eta_{22}=90$, and $\eta_{12}=\eta_{21}=70$.

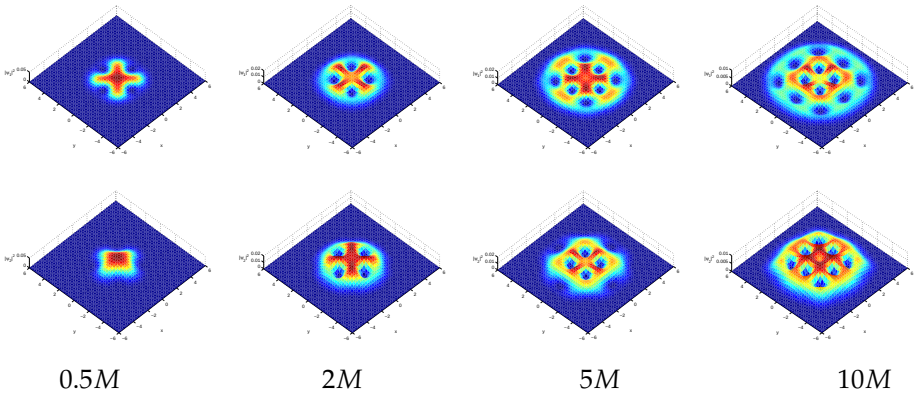

Figure 4: The contours of the ground state solutions of (1.3) with $P(\mathbf{x})=0$, upper: $|\psi_1|^2$, low: $|\psi_2|^2$, where $\omega=0.7$, $M=(\eta_{ij})$ with $\eta_{11}=110$, $\eta_{22}=90$, $\eta_{12}=\eta_{21}=70$, and various scales of M.

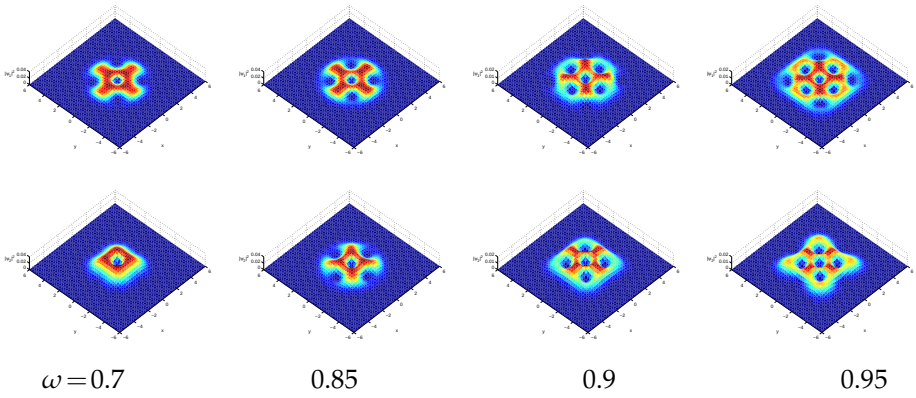

Figure 5: The contours of the first excited state solutions of (1.3) with $P(\mathbf{x})=0$, upper: $|\psi_1|^2$, low: $|\psi_2|^2$, where $\omega=0.7$, 0.8, 0.9, and 0.95, $\eta_{11}=110$, $\eta_{22}=90$, and $\eta_{12}=\eta_{21}=70$.

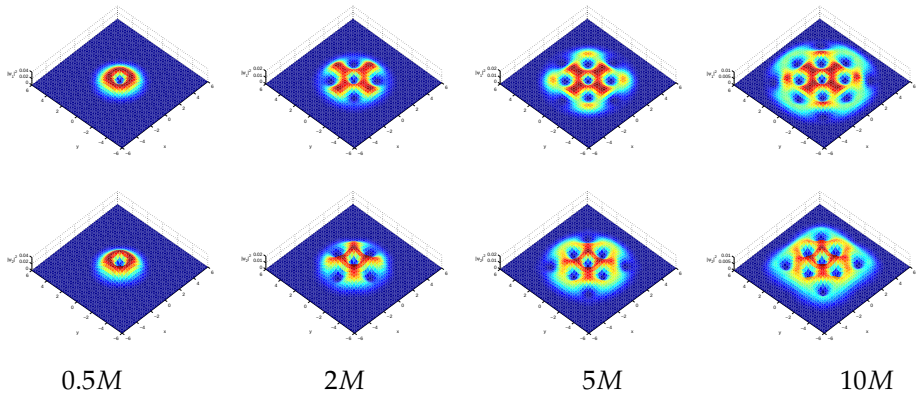

Figure 6: The contours of the first excited state solutions of (1.3) with $P(\mathbf{x})=0$, upper: $|\psi_1|^2$, low: $|\psi_2|^2$, where $\omega=0.7$, $M=(\eta_{ij})$ with $\eta_{11}=110$, $\eta_{22}=90$, $\eta_{12}=\eta_{21}=70$, and various scales of M.

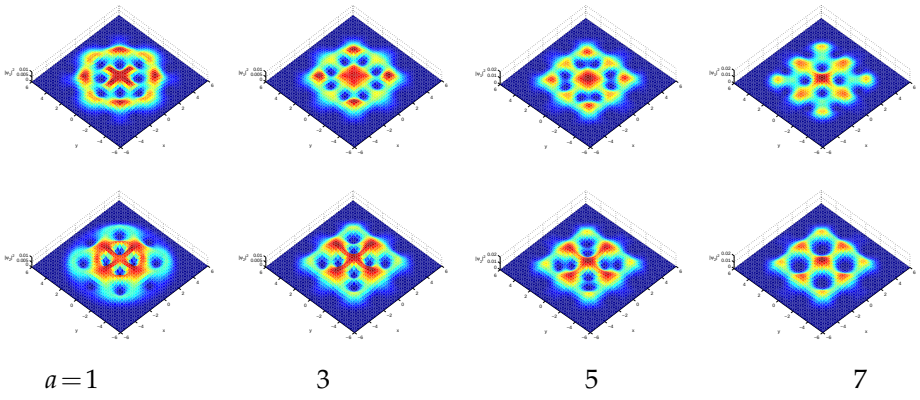

Figure 7: The contours of the ground state solutions of (1.3), upper: $|\psi_1|^2$, low: $|\psi_2|^2$, where $\omega=0.7$, $\eta_{11}=1100$, $\eta_{22}=900$, $\eta_{12}=\eta_{21}=700$, $d=3$, and various scales of a.

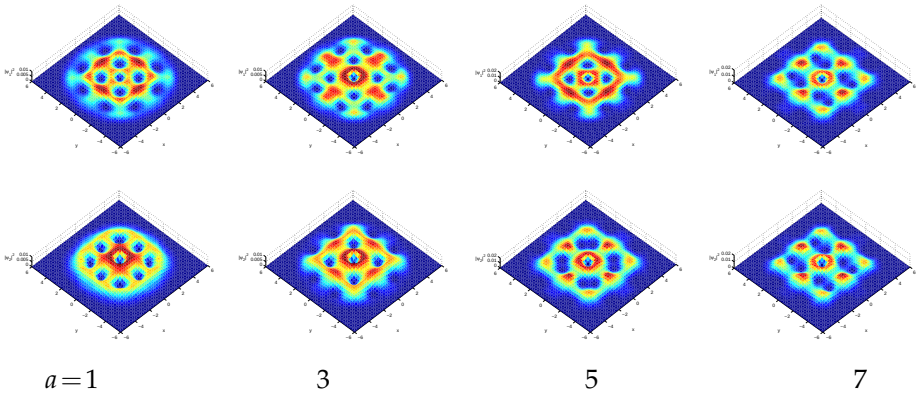

Figure 8: The contours of the first excited state solutions of (1.3), upper: $|\psi_1|^2$, low: $|\psi_2|^2$, where $\omega=0.7$, $\eta_{11}=1100$, $\eta_{22}=900$, $\eta_{12}=\eta_{21}=700$, $d=3$, and various scales of a.

Table 4: The first bifurcation points and associated energy levels of (1.3), where $\omega=0.7$, $\eta_{11}=1100$, $\eta_{22}=900$, $\eta_{12}=\eta_{21}=700$, and $d=3$.

a	1	3	5	7
$\lambda_{1,1}=\lambda_{2,1}$	1.6120	2.6411	3.5638	4.4440
$\lambda^*_{1,1}$	10.5138	12.4021	14.2589	16.0501
$\lambda^*_{2,1}$	10.4179	12.3636	14.2113	15.9738

Table 5: The second bifurcation points and associated energy levels of (1.3), where $\omega=0.7$, $\eta_{11}=1100$, $\eta_{22}=900$, $\eta_{12}=\eta_{21}=700$, and $d=3$.

a	1	3	5	7
$\lambda_{1,2}=\lambda_{2,2}$	2.2392	3.7519	4.9062	5.9082
$\lambda^*_{1,2}$	10.3578	12.3959	14.2240	15.9543
$\lambda^*_{2,2}$	10.3124	12.3888	14.2010	15.8673

functions $|\psi_1|^2$ and $|\psi_2|^2$ is clear when the value of $a_1=a_2=a$ is large. The number of peaks agree with the formula $\prod_{j=1}^{2}(12/d_j-1)$ in [17].

Example 4.5 (The first excited state solutions of rotating two-component BECs in optical lattices.)**.** We used the SCCM to trace the second solution curves of (1.3) where $\omega=0.7$, $\eta_{11}=1100$, $\eta_{22}=900$, $\eta_{12}=\eta_{21}=700$ and $d=3$. Fig. 8 shows the contours of the wave functions $|\psi_1|^2$ and $|\psi_2|^2$ with various values of a.

5 Conclusions

We have developed a two-parameter continuation algorithm combined with the SCM for computing numerical solutions of rotating two-component BECs and rotating two-component BECs in optical lattices, where the second kind Chebyshev polynomials were used as the basis functions for the trial function space. Based on the performance of the numerical methods we proposed and the numerical results, we wish to give some concluding remarks as follows.

(i) Since the two components ψ_1 and ψ_2 have different physical properties, the associated chemical potentials λ_1 and λ_2 are also different. Therefore, we must treat λ_1 and λ_2 as the different continuation parameters simultaneously. In addition, the classical unit tangent vector should be split into two unit tangent vectors of equal weight with respect to ψ_1 and ψ_2, and served as the constraint conditions. This fact has been verified by the numerical experiments.

(ii) The second kind Chebyshev polynomials can supply accurate numerical solutions for the GPE with exponential rate of convergence. See Table 1 and Fig. 1.

(iii) For the ground state solutions of rotating two-component BECs, Figs. 3-4 show that when the two components have the same number of vortices, the first component

has vortices at which the second component has peaks. The results are consistent with those in [11]. Moreover, as we increased the angular velocity from $\omega = 0.7$ to 0.95, the number of vortices also evolved gradually from 4 to 8. However, the two component may not have the same number of vortices if we use large scale of intra-component and inter-component interactions, where the inter-component interactions are the same. For instance, when we chose the interaction matrix equals $10M$, the first component has 12 vortices but the second one only has 8 vortices. See Table 2(b). The result is consistent with the report in [11], and is different from the prediction of Mueller *et al*. [5].

(iv) For the first excited state solutions of rotating two-component BECs, Figs. 5-6 show that the two components may not have the same number of vortices when the angular velocity $\omega = 0.7$ but the interaction matrix equals M or $10M$. See Table 3. Moreover, the number of vortices increased when we increased the angular velocity or used a large scale of interaction matrix, say $10M$, where the total number of particles approximately equals 10^6. Additionally, Figs. 5-6 also show that the first component has vortices at which the second component has peaks when they have the same number of vortices.

(v) In Examples 4.4-4.5 we studied the competition between the periodic potential and the cubic nonlinearities. The numerical results show that if the effect of the periodic potential is weak, the vortices in the ground state and first excited state solutions of a rotating two-component BECs in optical lattices are visible. As we increased the effect of the periodic potential, pairs of neighboring vortices of the two components gradually pinned together. When the effect of the periodic potential was strong enough, the vortices of the ψ_1 component remained unchanged, and those of the ψ_2 component became large.

Acknowledgments

The research was supported by the National Science Council of R.O.C. (Taiwan) through Project NSC 98-2115-M-231-001-MY3.

References

[1] K. W. Madison, F. Chevy, W. Wohlleben and J. Dalibard, Vortex formation in a stirred Bose-Einstein condensate, Phys. Rev. Lett., 84 (2000), 806-809.
[2] J. R. Abo-Shaeer, C. Raman, J. M. Vogels and W. Ketterle, Observation of vortex lattices in Bose-Einstein condensates, Science, 292 (2001), 476-479.
[3] P. C. Haljan, I. Coddington, P. Engels and E. A. Cornell, Driving Bose-Einstein-condensate vorticity with a rotating normal cloud, Phys. Rev. Lett., 87 (2001), 210403.
[4] E. Hodby, G. Hechenblaikner, S. A. Hopkins, O. M. Marago and C. J. Foot, Vortex nucleation in Bose-Einstein condensates in an oblate, purely magnetic potential, Phys. Rev. Lett., 88 (2002), 010405.
[5] E. J. Mueller and T.-L. Ho, Two-component Bose-Einstein condensates with a large number of vortices, Phys. Rev. Lett., 88 (2002), 180403.

[6] K. Kasamatsu, M. Tsubota and M. Ueda, Vortex phase diagram in rotating two-component Bose-Einstein condensates, Phys. Rev. Lett., 91 (2003), 150406.
[7] K. Kasamatsu, M. Tsubota and M. Ueda, Structure of vortex lattices in rotating two-component Bose-Einstein condenstates, Phys. B, 329-333 (2003), 23-24.
[8] K. Kasamatsu, M. Tsubota and M. Ueda, Vortex states of two-component Bose-Einstein condensates with and without internal Josephson coupling, J. Low Temp. Phys., 134 (2004), 719-724.
[9] K. Kasamatsu and M. Tsubota, Vortex sheet in rotating two-component Bose-Einstein condensates, Phys. Rev. A, 79 (2009), 023606.
[10] Y. Zhang, W. Bao and H. Li, Dynamics of rotating two-component Bose-Einstein condensates and its efficient computation, Phys. D, 234 (2007), 49-69.
[11] H. Wang, Numerical simulations on stationary states for rotating two-component Bose-Einstein condensates, J. Sci. Comput., 38 (2009), 149-163.
[12] J. C. Mason and D. C. Handscomb, Chebyshev Polynomials, Chapman & Hall/CRC, New York, 2003.
[13] J. Shen, T. Tang and L.-L. Wang, Spectral Method: Algorithms, Analysis and Applications, Springer Series in Computational Mathematics, New York, 2011.
[14] S.-L. Chang and C.-S. Chien, Adaptive continuation algorithms for computing energy levels of rotating Bose-Einstein condensates, Comput. Phys. Commun., 177 (2007), 707-719.
[15] Z.-C. Li, S.-Y. Chen, C.-S. Chien and H.-S. Chen, A spectral collocation method for a rotating Bose-Einstein condensation in optical lattices, Comput. Phys. Commun., 182 (2011), 1215-1234.
[16] Y.-S. Wang and C.-S. Chien, A spectral-Galerkin continuation method using Chebyshev polynomials for the numerical solutions of the Gross-Pitaevskii equation, J. Comput. Appl. Math., 235 (2011), 2740-2757.
[17] H.-S. Chen and C.-S. Chien, Multilevel spectral-Galerkin and continuation methods for nonlinear Schrödinger equations, SIAM J. Multiscale Model. Simul., 8 (2009), 370-392.
[18] C.-S. Chien, S.-L. Chang and B. Wu, Two-stage continuation algorithms for Bloch waves of Bose-Einstein condensates in optical lattices, Comput. Phys. Commun., 181 (2010), 1727-1737.
[19] C.-S. Chien, S.-L. Chang and Z. Mei, Tracing the buckling of a rectangular plate with the block GMRES method, J. Comput. Appl. Math., 136 (2001), 199-218.
[20] Y.-C. Kuo, W.-W. Lin, S.-F. Shieh and W. Wang, A minimal energy tracking continuation method for coupled nonlinear Schrödinger equations, J. Comput. Phys., 228 (2009), 7941-7956.
[21] S.-M. Chang, Y.-C. Kuo, W.-W. Lin and S.-F. Shieh, A continuation BSOR-Lanczos-Galerkin method for positive bound states of a multi-component Bose-Einstein condensate, J. Comput. Phys., 210 (2005), 439-458.
[22] J.-H. Chen, I.-L. Chern and W. Wang, Exploring ground states and excited states of spin-1 Bose-Einstein condensates by continuation methods, J. Comput. Phys., 230 (2011), 2222-2236.
[23] G. L. Alfimov and D. A. Zezyulin, Nonlinear modes for the Gross-Pitaevskii equation-a demonstrative computation approach, Nonlinearity, 20 (2007), 2075-2092.
[24] D. A. Zezyulin, G. L. Alfimov, V. V. Konotop and V. M. Péréz-Garcia, Control of nonlinear modes by scattering-length management in Bose-Einstein condensates, Phys. Rev. A., 76 (2007), 013621.
[25] D. A. Zezyulin, G. L. Alfimov, V. V. Konotop and V. M. Péréz-Garcia, Stability of excited states of a Bose-Einstein condensates in an anharmonic trap, Phys. Rev. A., 78 (2008), 013606.

[26] S.-L. Chang, C.-S. Chien and B.-W. Jeng, Computing wave functions of nonlinear Schrödinger equations: A time-independent approach, J. Comput. Phys., 226 (2007), 104-130.
[27] G. H. Golub and C. F. Van Loan, Matrix Computations, 3rd ed., The Johns Hopkins Univ. Press, Baltimore, 1996.
[28] E. L. Allgower and K. Georg, Introduction to Numerical Continuation Methods, Society for Industrial and Applied Mathematics (SIAM), Philadelphia, PA, 2003.
[29] H. B. Keller, Lectures on Numerical Methods in Bifurcation Problems, Springer, Berlin, 1987.
[30] T. F. Chan, Deflation techniques and block-elimination algorithm for solving Bordered singular system, SIAM J. Sci. Statist. Comput., 5 (1984), 121-134.
[31] P. J. Budden and J. Norbury, A nonlinear elliptic eigenvalue problem, J. Inst. Math. Appl., 24 (1979), 9-33.
[32] C.-S. Chien and B.-W. Jeng, A two-grid discretization scheme for semilinear elliptic eigenvalue problems, SIAM J. Sci. Comput., 27 (2006), 1287-1304.